Arch. Metall. Mater. **65** (2020), 2, 627-638

DOI: 10.24425/amm.2020.132802

M.R. MAJDI[1], I. DANAEE[1*], D. ZAAREI[2], M. FARZAM[1]

IMPROVEMENT OF MICROSTRUCTURE AND BARRIER PROPERTIES OF SILICATE COATINGS ON LOW CARBON STEEL BY INCORPORATING COLLOIDAL NANO-SiO_2

Silicate coatings have been considered as an alternative to toxic and carcinogenic other chemical treatments. In this paper, a strengthened silicate coating was formed on the surface of low carbon steel by dip immersion method. The modification and strengthening was done by loading colloidal nano-SiO_2 into the film. The characterizations of nano-SiO_2 were investigated by FESEM, TEM and FT-IR. The effects of nano contents (weight ratio) and drying temperatures on corrosion properties of silicate film were studied. Potentiodynamic polarization, electrochemical impedance spectroscopy and immersion tests have been used to study corrosion behavior of nano-loaded silicate films. Surface morphology, microstructure and its chemical composition were analyzed by means of FESEM, EDS, AFM, XRD, GIXRD, ATR-FTIR and Raman techniques. Results indicated that colloidal nano-SiO_2 properly modified the silicate coatings and significantly improved the corrosion resistance and barrier property. Also drying temperature showed a considerable effect in silicate coating and higher corrosion resistance was obtained with 150°C curing.

Keywords: Colloidal Nano-SiO2, Silicate coatings, Corrosion, AFM, ATR-FTIR

1. Introduction

Carbon and low-alloy steels are the most extensively used materials in industries because of their low cost and good mechanical properties. But, this metal has a limited corrosion resistance and therefore the corrosion of carbon steels is a problem for most industries [1,2]. Therefore, many efforts have been done to increase corrosion resistance and stability of steel materials [3,4]. There are different corrosion protection methods including cathodic/anodic protection, coatings, inhibitors and proper design [5-8]. Surface treatment is a generic way to protect metals from corrosion, which includes physical vapor deposition, chemical conversion coating, electroless and electroplating and so on [9,10]. Between these surface coatings, chemical conversion treatments are the cost effective and simple method and have been effectively employed in a wide range of applications [11-13]. Silicate coating is one of the most promising treatments which can be the alternatives to the hexavalent chromium [14-16].

The soluble silicates are environmentally friendly and economically beneficial materials. Silicate solutions are complex mixtures of silicate anions which are created by condensation of $Si(OH)_4$. Thus, the silicate tetrahedron is the fundamental unit forming the silicate anions. In a silicate structure, the *n* number of SiO_4^{4-} units is connected to a silicate tetrahedron. Therefore, a silicate solution contains silicate monomers and polymeric particles and moreover, its anionic complexity is caused by the solution properties such as silicon to cation ratio and concentrations [17,18]. The interactions of soluble silicates with metals have been previously studied in literatures [19-24]. Silanol groups (SiOH) form hydrogen bonds in contact with hydroxyl-covered metallic surfaces. Upon drying, the condensation reaction occurs leading to metallo-siloxane bonds formation (Me-O-Si) and increasing the adherence of the silicates to the metallic substrates. In addition, the siloxane bond (Si-O-Si) network is generated by the excess of the SiOH group in the adsorbed structure and hinders the diffusion of the aggressive ions to coating layer [25-27]. Gaggiano et al. [28] suggested that the cations Na^+, K^+, Li^+ have effective role in deposition mechanism and act as a coagulating agent between the surface and the silicate anionic structures in solution. Existence of cracks, micropores and areas with low cross-link density affects the long-term corrosion protection of silicate layer. These defects facilitate the penetration of corrosive electrolyte to the substrate/coating interface and are preferential sites for corrosion protection [29,30]. In recent years many attempts have been done to modify the silicate layer by incorporation of corro-

[1] UNIVERSITY OF TECHNOLOGY, ABADAN FACULTY OF PETROLEUM ENGINEERING, PETROLEUM ABADAN, IRAN
[2] ISLAMIC AZAD UNIVERSITY, TECHNICAL FACULTY, SOUTH TEHRAN BRANCH, TEHRAN, IRAN

* Corresponding author: danaee@put.ac.ir

sion inhibitors, nano-particles and other additives to the coating bath [31,32]. Deposition of silicate films has been previously accomplished by several methods over wide range of metallic substrates including zinc, copper, galvanized steel, aluminum and its alloys [32,33]. However, electrochemical behavior and characteristics of silicate layer on carbon steel isn't clear yet.

In the present work, the deposition and modification of silicate layer by colloidal nano silica on the surface of steel was investigated. Characterization of nano silica particles were studied by Transmission electron microscopy, field emission scanning electron microscopy and fourier transformed infrared spectroscopy. The corrosion protection behavior of silicate coatings was evaluated by Tafel polarization, immersion test and impedance spectroscopy. The morphology of silicate coatings were investigated by FESEM and atomic force microscopy (AFM). Moreover, the elemental and structural analysis of the coatings was investigated by grazing incident X-ray diffraction analysis (GIXRD), energy-dispersive spectroscopy (EDS) and attenuated total reflection Fourier transformed infrared (ATR-FTIR) spectroscopy.

2. Experimental

2.1. Sample preparation

The Steel samples were polished with abrasive papers (400-2000 mesh), and then cleaned with acetone. The samples were degreased for 30 s in a 1 M NaOH solution and then rinsed with water. A 18 wt.% aqueous solution of colloid nano-SiO_2 with 15-20 nm particle size was purchased from Iranian Nanomaterials Pioneers Company. A 50 wt.% aqueous solution of potassium silicate was purchased from the Iran Silis Company. Coating solutions with different weight ratios were prepared by mixing silicate and nano-SiO_2 in different ratio. Pretreated steel samples were coated by immersing in the coating bath at room temperature for 7 min. The coated samples were then dried in the furnace for 30 min to obtain an extensively cross-linked film structure.

2.2. Characterization

Potentiostat/galvanostat model PGSTAT 302N was used for electrochemical experiments including platinum sheet, Ag/AgCl, and low carbon steel as counter, reference and working electrode, respectively in 3.5 wt% NaCl solutions. For polarization tests, the potential was swept at a rate of 1 mV s^{-1} and corrosion parameters were obtained by Tafel extrapolation method. Impedance experiments were carried out with AC amplitude 10 mV at open circuit potential (OCP) and frequency sweep from 100 kHz to 100 mHz. Impedance data were fitted to the electrical equivalent circuit and impedance parameters were calculated. Corrosion behavior of silicate coatings was also evaluated by immersion test according to ASTM D6943. The morphology of the nano-silica and silicate coatings was observed using field emission scanning electron microscopy (FESEM) model TESCAN/MIRA3 and atomic force microscopy (AFM) model NanoSurf easyscan 2. The structure and chemical composition of coatings were investigated by energy dispersive spectroscopy, X-ray diffraction analysis (XRD) and grazing incident X-ray diffraction analysis (GIXRD) model PHILIPS PW1730 and attenuated total reflection fourier transformed infrared spectroscopy (ATR-FTIR) model Thermo AVATAR.

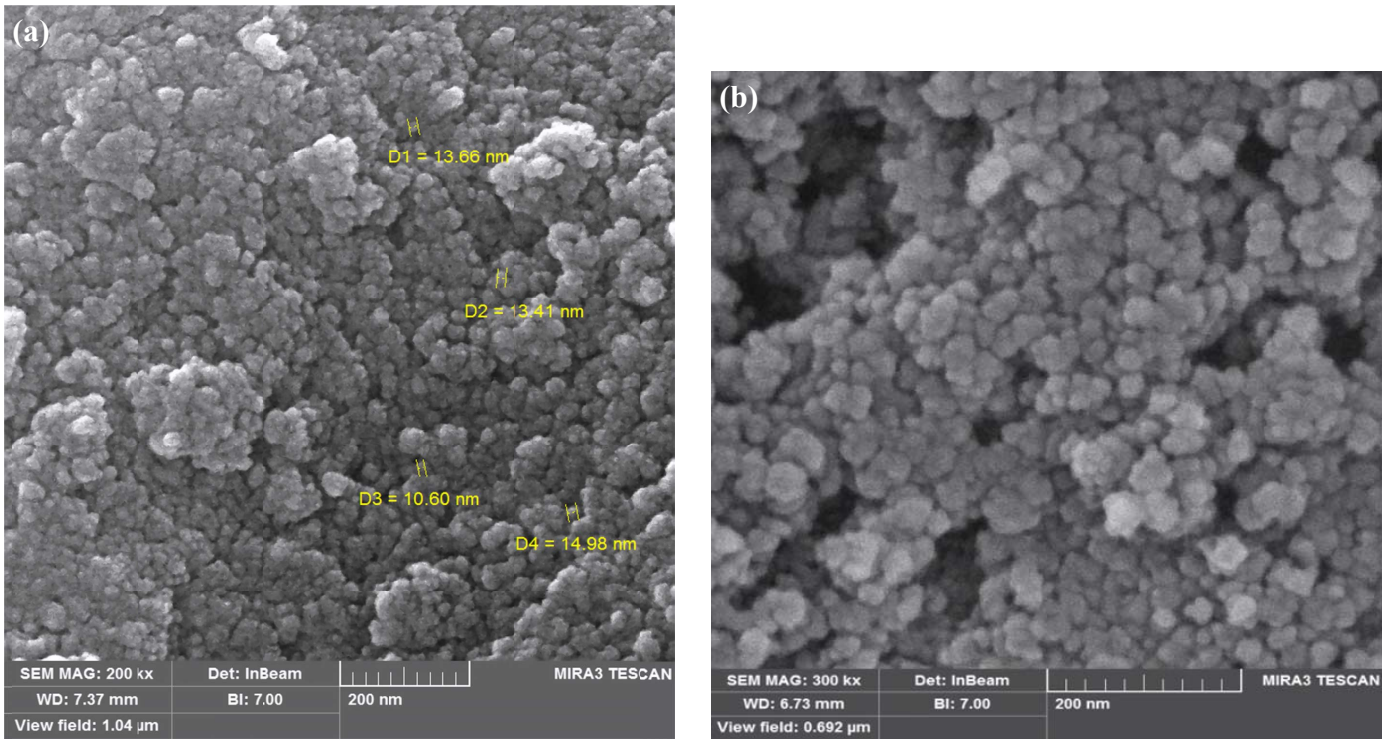

Fig. 1. (a) FESEM images of Nano silica in different magnification, (a) 200 kx and (b) 300 kx

3. Results and discussion

3.1. Characterization of Nano-silica

Figure 1 shows the FESEM images of nano-silica in different magnifications. As can be seen, the size of nano particles is around 20 nm which increases the possibility of contribution to silicate coatings structure. Figure 2 shows the TEM image of colloidal nano-silica which is in agreement with FESEM images and indicates that the nano particles are suitably separated.

Figure 3 presents the FT-IR spectroscopy of nano-silica. In this diagram, the peaks at 484 and 810 cm^{-1} are due to Si-O and Si-OH bonds, respectively. Moreover, a broad peak at 1150 cm^{-1} is related to the asymmetric Si-O-Si stretching vibration [21,34,35]. The peak at 3480 cm^{-1} is generated by stretching vibration of -OH groups.

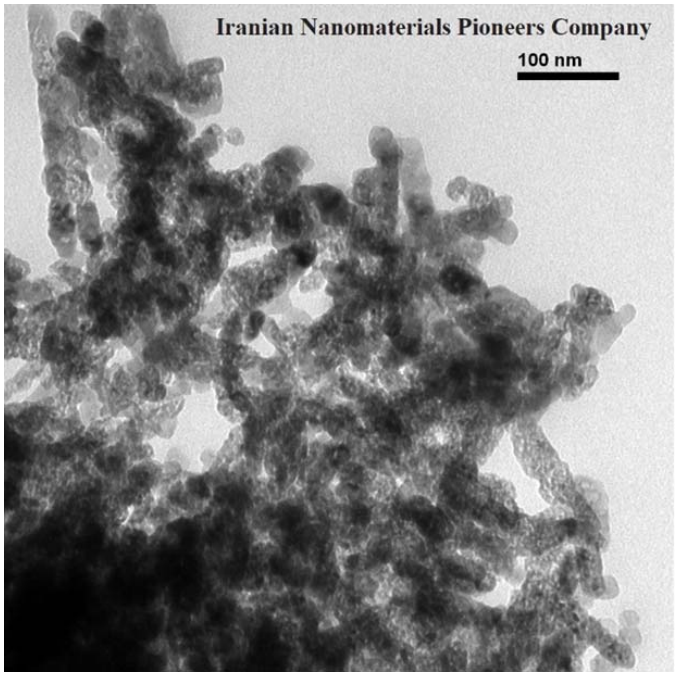

Fig. 2. TEM image of colloidal nano SiO_2

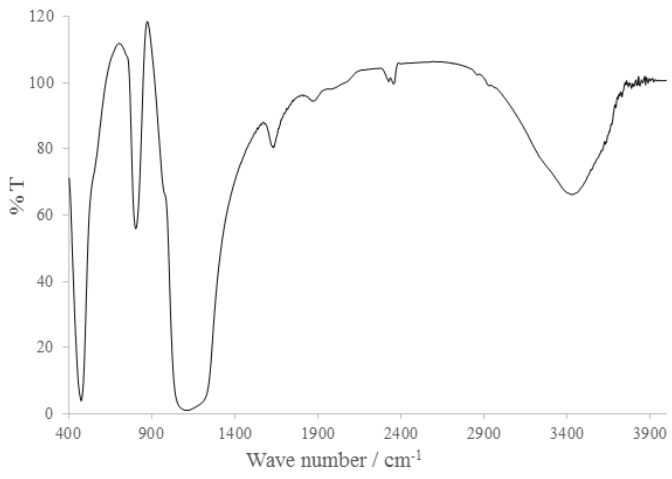

Fig. 3. FTIR spectra of colloid nano-SiO_2

3.2. Corrosion tests

The tafel polarization curves of bare carbon steel and silicate coatings in 3.5 wt.% NaCl solution are shown in Fig. 4. Coatings loaded with different amount of colloidal nano particles, were prepared by 7 min dip immersion in silicate coating solutions and then cured in 150°C for 30 min. Tafel parameters were calculated and listed in Table 1. It can be seen that by applying unloaded silicate film, both anodic and cathodic branches of polarization curve shift toward the direction where the corrosion current decreases, suggesting that the anodic and the cathodic process of steel corrosion are inhibited simultaneously. The development in the corrosion protection is due to the formation of the fully cross-linked silicate film through the heat treatment process.

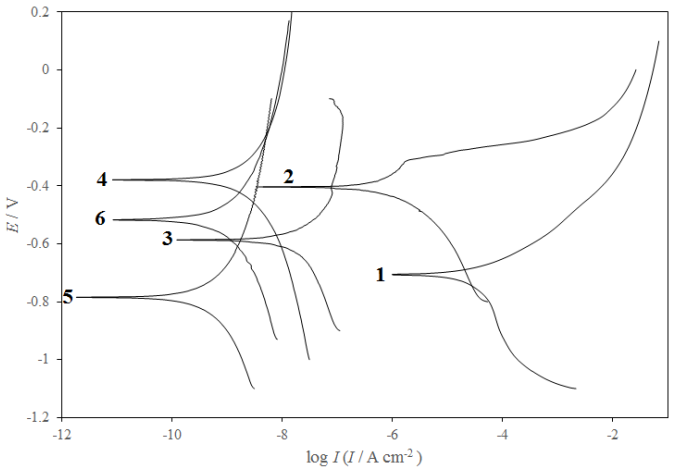

Fig. 4. Polarization curves of the low carbon steel and silicate coatings in 3.5 wt.% NaCl solution. Coatings were prepared by 7 min immersion time in silicate bath with different ratio and then drying at 150°C for 30 min. (1) Bare, (2) ratio 1.7, (3) ratio 2.1, (4) ratio 2.5, (5) ratio 2.9 and (6) ratio 3.3

Adding colloidal nano-SiO_2 effectively increases the weight ratio, thereby causing more complex polymers to form. Silicates with higher weight ratios have more polymeric units in the liquid silicate, so have a higher probability of forming Si-O-Si bonds between particles during drying [36,37]. More polymeric units in the liquid state will lead to a more close packed structure in the dehydrated structure. As can be seen in Fig. 4 and Table 1, by increasing the ratio up to 2.9, corrosion resistance increases and I_{corr} of coated samples significantly decreases. Furthermore, FTIR spectrum of the colloid nano-SiO_2 (Fig. 1d) shows that silanol groups exist in its structure. Therefore, upon drying, colloidal silica contributes through condensation reaction and connects to the silicate structure. Thus, nano particles fill the vacant spaces and pores in the silicate network due to its small size and improvement in barrier properties can be obtained. Silica particles have a negative charge and are attracted to the hydrophilic site of the silicate compound [38]. The bonding of the silica to the positively charge site removes this site as a possible water molecule bonding site on the silicate film. As a result, less water bonding sites are available thereby transition into the

TABLE 1

Electrochemical parameters of silicate coatings with different ratio in 3.5 wt.% NaCl solution.
Coatings were prepared in 7 min immersion time, 150 °C drying temperature and 30 min drying time

Sample	E_{corr} / V	I_{corr} / A cm^{-2}	β_a / V dec^{-1}	β_c / V dec^{-1}	R_p / ohm	V_{corr} / mm y^{-1}
Bare steel	–0.706	1.21×10^{-5}	0.061	0.101	$1.36\times10^{+3}$	1.31×10^{-1}
Silicate coatings (ratio 1.7)	–0.403	1.04×10^{-7}	0.028	0.025	$5.51\times10^{+4}$	1.13×10^{-3}
Nano-modified silicate (ratio 2.1)	–0.586	3.59×10^{-9}	0.05	0.052	$3.08\times10^{+6}$	3.91×10^{-5}
Nano-modified silicate (ratio 2.5)	–0.379	4.72×10^{-10}	0.08	0.085	$3.79\times10^{+7}$	5.13×10^{-6}
Nano-modified silicate (ratio 2.9)	–0.785	9.49×10^{-11}	0.073	0.07	$1.63\times10^{+8}$	1.03×10^{-6}
Nano-modified silicate (ratio 3.3)	–0.487	1.51×10^{-10}	0.062	0.056	$8.52\times10^{+7}$	1.63×10^{-6}

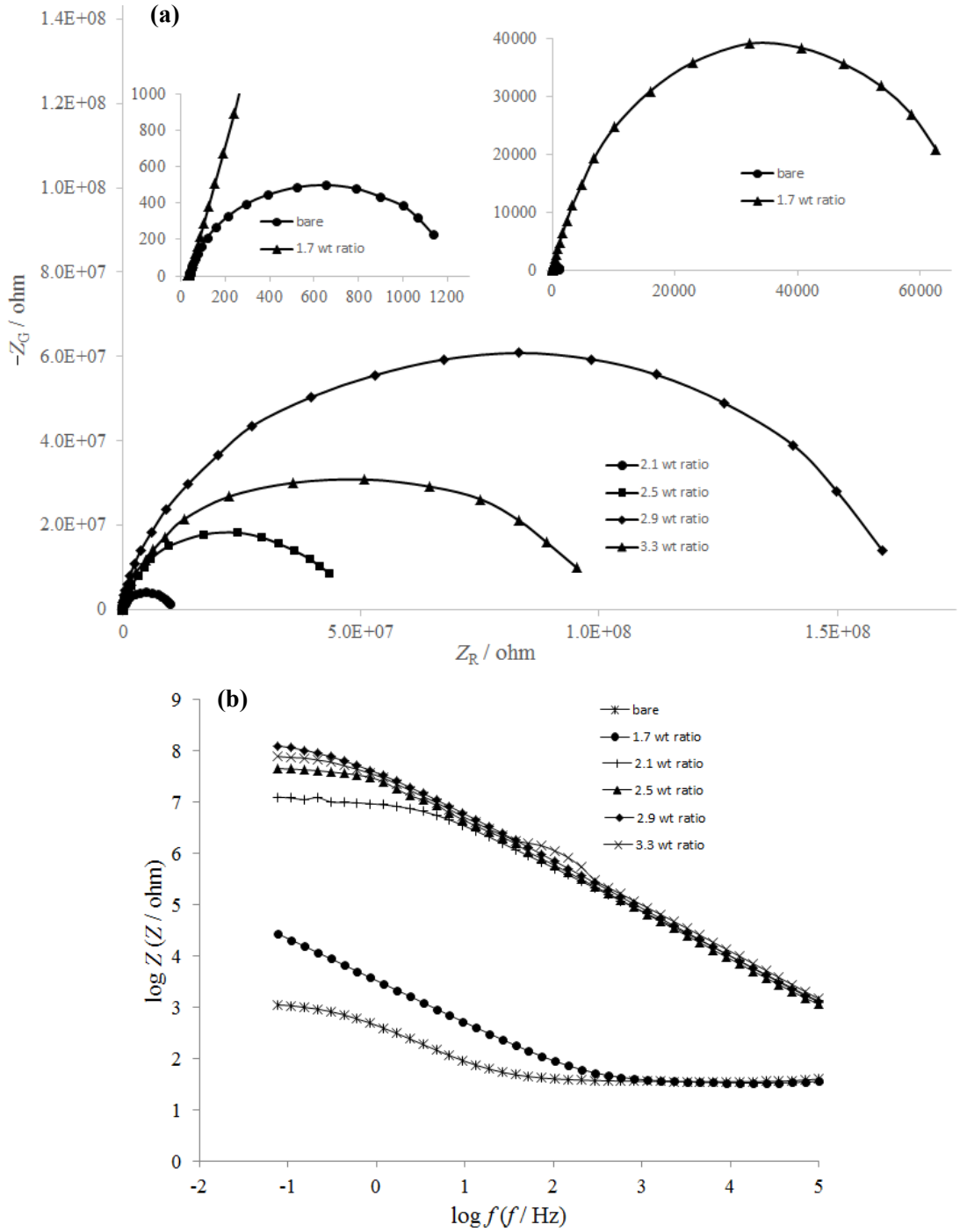

Fig. 5. Electrochemical impedance spectroscopy diagrams of the low carbon steel and silicate coatings in 3.5 wt.% NaCl solution. Coatings were prepared by 7 min immersion time in silicate bath with different ratio and then drying at 150°C for 30 min. (1) Bare, (2) ratio 1.7, (3) ratio 2.1, (4) ratio 2.5, (5) ratio 2.9 and (6) ratio 3.3

coating being less possible. In addition, the silicon on the silica can bond with the oxygen on the silicate compound. The silicon bonding to the oxygen can result in blocking of potentially available water binding sites and/or the removal of potentially available water molecule binding sites on the silicate film [39].

In the higher ratio 3.3, the corrosion rate enhances negligibly and the protection behavior reduces. The aggregation of nanoparticles on the surface and limitations against the activity of these particles could be considered as a reason for this phenomenon. Thus, these particles could not play their effective roles to improve the continuity and hydrophobia properties of silicate layer [38-40].

Polarization resistances are calculated by Stern-Geary equation [13,14] in Table 1. As can be seen, highest polarization resistance is obtained for ratio 2.9, and decreases in higher ratio. The calculated polarization resistance values are in agreement with impedance values which confirm the applicability of destructive and non-destructive test for analyzing these coatings.

Impedance spectroscopy was applied to confirm the anticorrosion behavior of the silicate coatings. The nyquist and bode diagrams of nano-loaded silicate films deposited on steel are presented in Figure 5. The results were obtained in 3.5 wt.% NaCl solution at open circuit potential. The total impedance values of all silicate coatings are higher than that of bare steel. In addition, resistance of coatings increases with increasing the ratio up to 2.9 but decrease for the higher nano content. This is in a good agreement with the results of Tafel polarization. Silicate coatings formed on low carbon steel could be also explained by equivalent circuit showed in Fig. 6. In the proposed equivalent circuit, Q_c is a constant phase element corresponding to the capacitance containing double layer and coating capacitances $Q_c = R^{n-1} C_c^n$, R_s is solution resistance, and R_p is the polarization resistance which includes film resistance, charge transfer resistance, accumulation resistance and double layer resistance. In the equivalent circuit, the capacitor (C) was replaced with a constant phase element (CPE) Q due to the micro and nano roughness of silicate coating surfaces [41,42]. The circuit elements were calculated by fitting the experimental impedance data to the electrical equivalent circuit (Table 2). As observed, carbon steel sample without treatment shows very low polarization resistance and high capacitance. The R_p values of bare carbon steel and silicate coatings are in good accordance with R_p in potentiodynamic polarization. The R_p value for ratio 2.9 is considerably higher than other silicate-treated samples, which is related to the existence of a most compact and faultless coating on the surface of steel. In addition, the capacitance values decreases with increasing nano content. This is due to the decrease in local dielectric constant in the presence of nanoparticles which fill the pores and inhibit water diffusion to the coatings. Water has a higher dielectric constant with respect to coating.

The surface images of the silicate samples after 168 h exposure in 5 wt% NaCl solution are presented in Fig. 7. As can be seen, unmodified silicate layer corrodes due to electrolyte penetration to the substrate and oxidation of the steel substrate begins and subsequently the "red rust" appears on the surface.

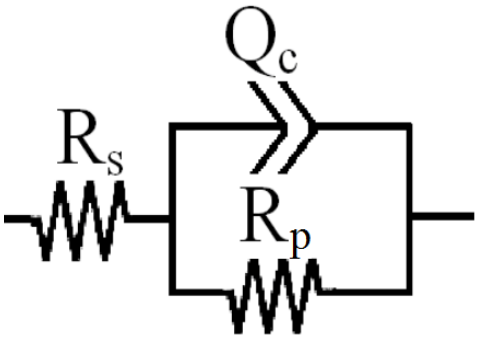

Fig. 6. Equivalent circuit compatible with the Nyquist diagram of silicate coated steel samples

TABLE 2

Impedance parameters for silicate coatings with different ratio using the equivalent circuit in Fig. 6. Coatings were prepared in 7 min immersion time, 150 °C drying temperature and 30 min drying time

Sample	Q_c / F	R_p / Ω	n
Bare steel	9×10^{-4}	$1.22\times10^{+3}$	0.85
Silicate coatings (ratio 1.7)	3×10^{-4}	$6.53\times10^{+4}$	0.95
Nano-modified silicate (ratio 2.1)	4×10^{-8}	$1.07\times10^{+7}$	0.85
Nano-modified silicate (ratio 2.5)	2×10^{-8}	$4.92\times10^{+7}$	0.75
Nano-modified silicate (ratio 2.9)	9×10^{-9}	$1.68\times10^{+8}$	0.79
Nano-modified silicate (ratio 3.3)	7×10^{-10}	$9.57\times10^{+7}$	0.73

By loading nano-particle, coating exhibits more corrosion resistance and no sign of corrosion and rusting can be observed on its surface. According to these pictures can be concluded that nano-silica has important role on corrosion protection of silicate layer and nano-SiO_2 was an excellent reinforcing agent and modifier for silicate coating.

3.3. Characterization of silicate coatings

Fig. 8 shows the FESEM images of silicate coating in different magnifications. As can be seen, the unmodified silicate coating contains discontinuities, agglomerates and cracks (Fig. 8a-c). These coating defects are the susceptible sites for the attack of corrosive ions and thus decrease the corrosion resistance. The corresponding EDS spectrum of silicate coatings is presented in Fig. 9. According to EDS and the elemental weight percent in Table 3, the Si:K weight ratio in silicate coatings is 0.73.

TABLE 3

Elemental analysis of silicate and Nano-modified silicate coatings by EDS

	O (w%)	O (A%)	Si (w%)	Si (A%)	K (w%)	K (A%)
Silicate coating with ratio 1.7	61.25	76.81	16.40	11.71	22.35	11.48
Nano-modified silicate coating with ratio 2.9	64.36	77.67	24.42	16.79	11.22	5.54

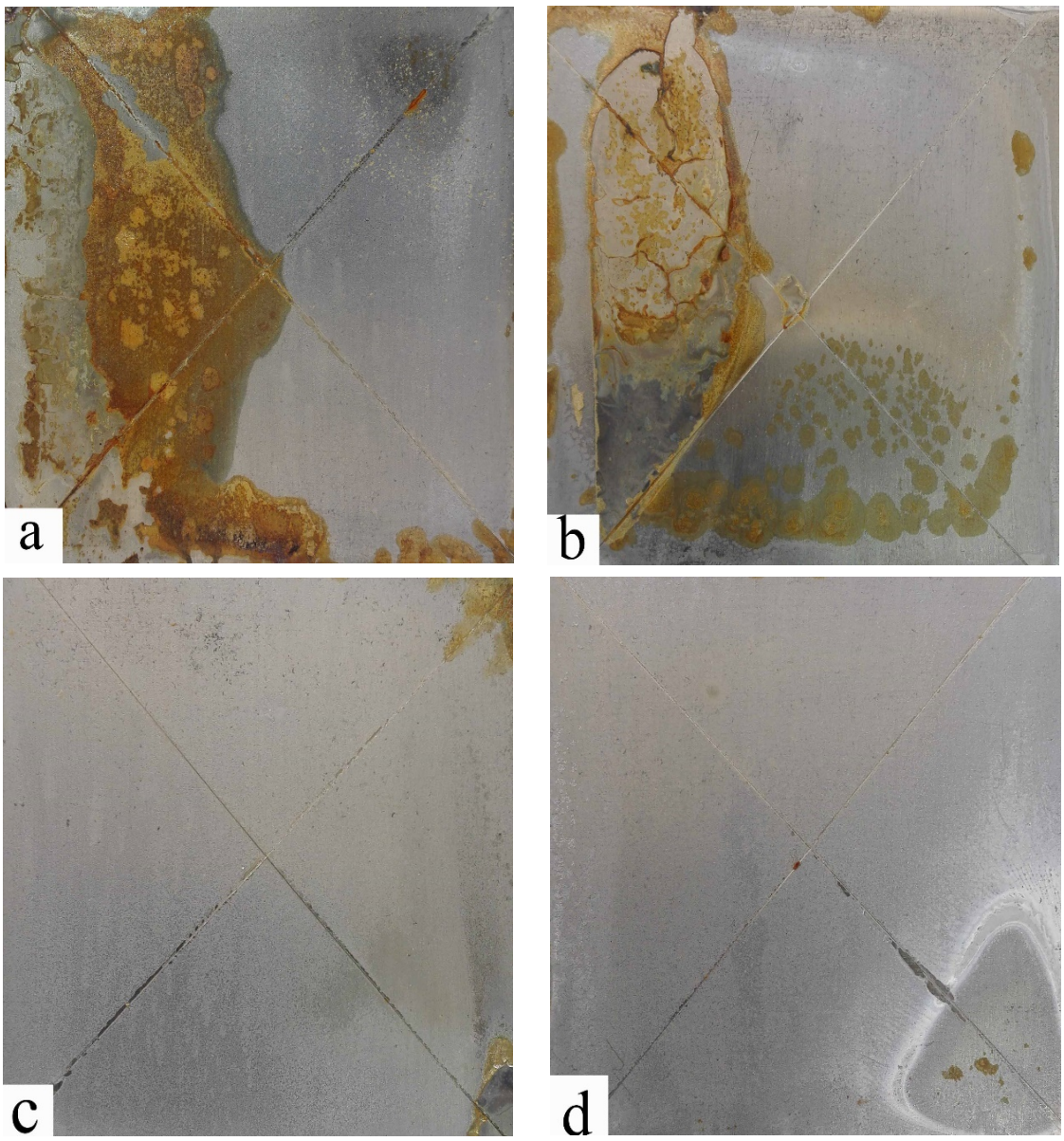

Fig. 7. Surface images of silicate coatings with different ratio (a) ratio 1.7, (b) ratio 2.1, (c) ratio 2.5, (d) ratio 2.9 after 168 h immersion in 5 wt% NaCl solution

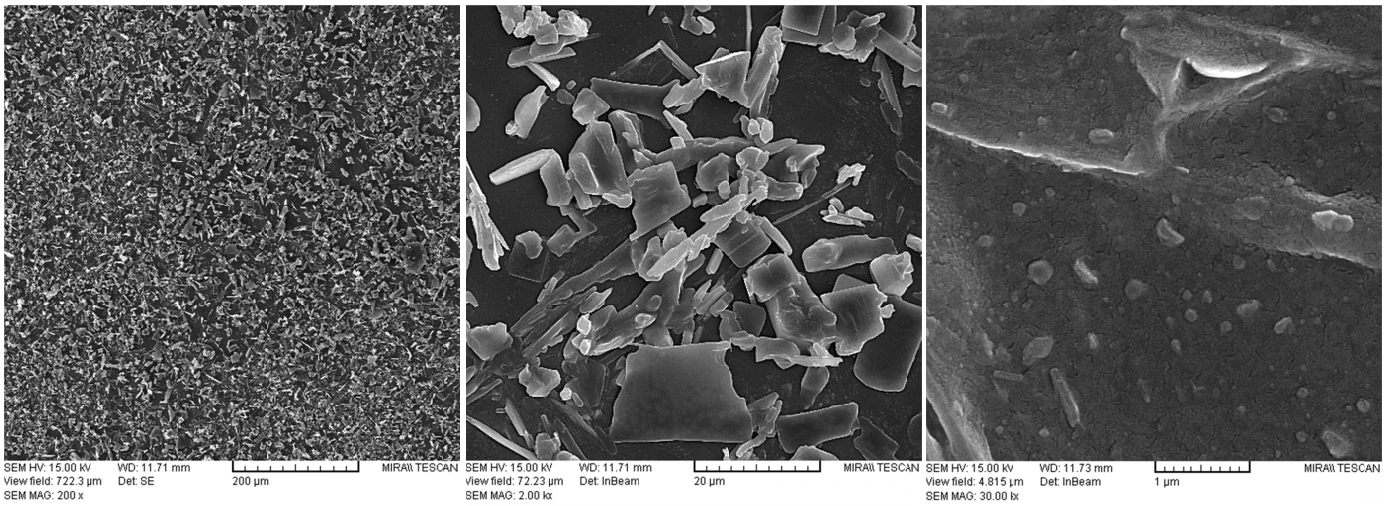

Fig. 8. FESEM images of silicate coating with ratio 1.7 in different magnifications. Coating was prepared by 7 min immersion time and then curing in 150°C for 30 min

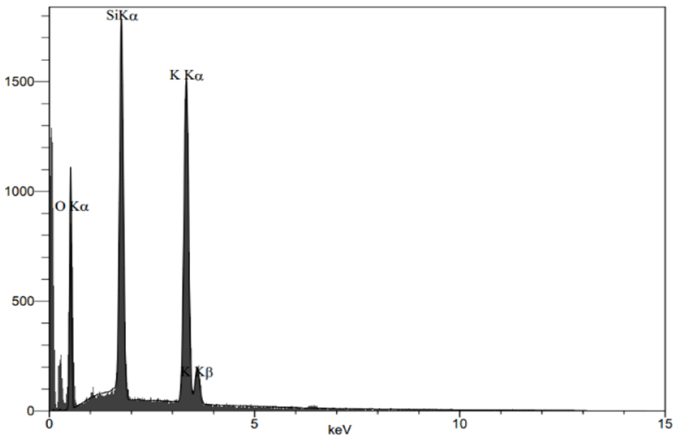

Fig. 9. EDS analysis of silicate coating with ratio 1.7

Fig. 10 illustrates the elemental mapping of silicate coating. It can be seen that silicon, potassium and oxygen is uniformly distributed in coating. Moreover, potassium is increased in agglomerates and external growth area.

Fig. 11 depicts the FESEM images of nano modified silicate coating in different magnifications. Surface of this coating is homogeneous and have lower agglomerates, cracks and irregularities in comparison with silicate coating. The crack in the silicate coatings occurs during heat treatment process which decreases the volume of the film by water evaporation and OH polycondensation reactions. The decrease in silicate film volume in shrinkage step and cross-linking, enhances the coating stress, and thus the cracks are created. Moreover, the cracks in silicate coating can be related to the cooling down step. The silicate coating and the metal substrate have different thermal expansion coefficient. According to the Fig. 11c, the decrease in cracks is observed in the modified silicate coating related to the loading of the nano-colloidal silica. Nano particles fill the pores and vacant spaces in silicate structure therefore the shrinkage of the nanoparticles-loaded silicate coating is lower than the shrinkage in the unmodified silicate coating, which causes the reduction in stress and cracks in the silicate film.

EDS data collected over the whole surface of the sample and presented in Fig. 12 and Table 3. As seen, the main elements

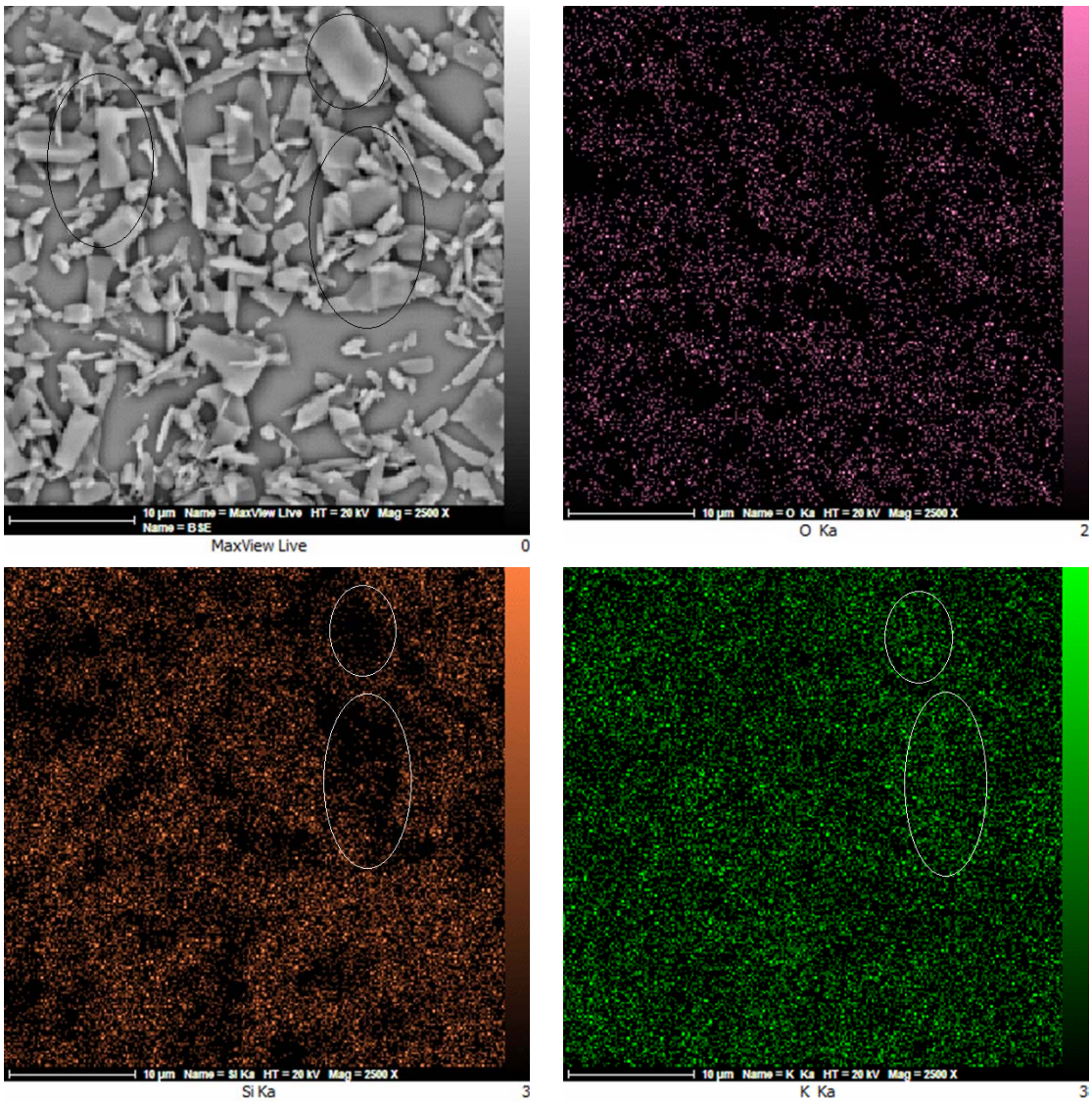

Fig. 10. Map analysis of silicate coating with ratio 1.7. Coating was prepared by 7 min immersion time and then curing in 150°C for 30 min

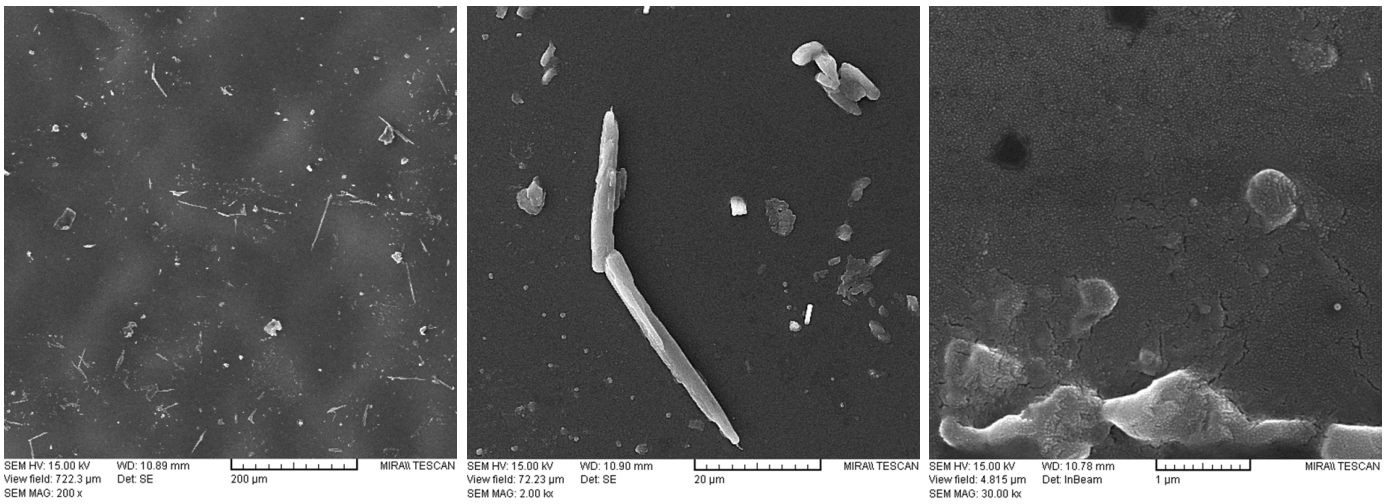

Fig. 11. FESEM images of nano-modified silicate coating with ratio 2.9 in different magnifications. Coating was prepared by 7 min immersion time and then curing in 150°C for 30 min

composed the coating layer on the steel substrates are Si, O, K. The results show that the Si/K weight ratio enhances for nano-silica modified silicate coating to 2.17.

Fig. 13 presents the elemental mapping of silicate coating with ratio 2.9. It is observed that that the distribution of silicon, potassium and oxygen is more uniform in coating. Moreover, the density of potassium and agglomerates are decreased and in addition the presence of Si is strongly increased.

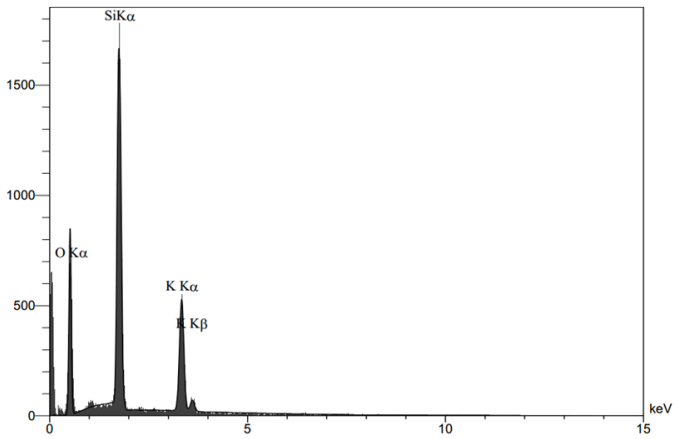

Fig. 12. EDS analysis of nano-silicate coating with ratio 2.9

Fig. 14 and 15 indicates the AFM images of silicate and nano modified coatings. Topography of different coatings shows a significant difference in surface roughness and typical surface features. Silicate coating shows appearance of agglomerates and large nodules on the surface. By loading the silica nano-particles into the silicate film, more uniform coating is obtained and the propensity of appearance of nodules in coating and the surface roughness decrease.

Fig. 16 presents the normal XRD pattern of silicate and nano-modified silicate coatings in the range $15° < 2\theta < 85°$. As can be seen, the recorded sharp peaks at 2θ of 44.9°, 65.2° and 82.5° are related to body-centered cubic (BCC) structure oriented in (110), (200) and (211) directions of iron and clear peaks at 2θ of 24.2°, 29.9°, and 34.1° refer to potassium silicate compounds. A lump with poor intensity is observed in 20° to 35°, which is due to the presence of disordered silicate film [34,43]. In the presence of nano-particles, the intensity of iron peaks decrease, also silicate peak increases. Because the silicate layer is thin and amorphous, identification of silicate with normal XRD is too difficult. Fig. 17 shows the GIXRD patterns from silicate and nano-modified silicate coatings. In both of GIXRD analysis observed that the silicate films are amorphous and crystalline phase is not observed [44].

Attenuated total reflection fourier transformed infrared (ATR-FTIR) spectroscopy was used to investigate the structure of silicate coatings. Fig. 18 presents the ATR-FTIR spectra of silicate and nano-modified coatings in the wavenumber region 1210-720 cm^{-1}. As can be seen, the broad peak at 900 to 1150 cm^{-1} is obtained which is related to the asymmetric Si-O-Si stretching vibration. In addition, the vibration band of Si-O-Si at 1000 cm^{-1} becomes more intensive in the presence of nano particles. More cross-links in silicate coating are generated in the presence of nano-silica, and thus more siloxane bonds can be created.

Fig. 19 presents the Raman spectroscopy of silicate and nano-modified coatings. The peak located at 413 is related to Si-O-Si bending mode and the peaks at 627 and 1020 are related to symmetric stretching vibrations of Si-O and Si-OH, respectively [45,46]. It is observed that the peaks are negligible due to the thin layer of silicate coating but become more intensive in the presence of nano-particles. This indicates that more silicate bonds are created with colloidal nano-silica.

3.4. Effect of drying temperature

Fig. 20 shows the potentiodynamic polarization diagrams of nano-modified silicate coated steel with ratio 2.9 which prepared in different curing temperatures. Also, the calculated corrosion parameters are illustrated in Table 4. As seen, I_{corr} and corro-

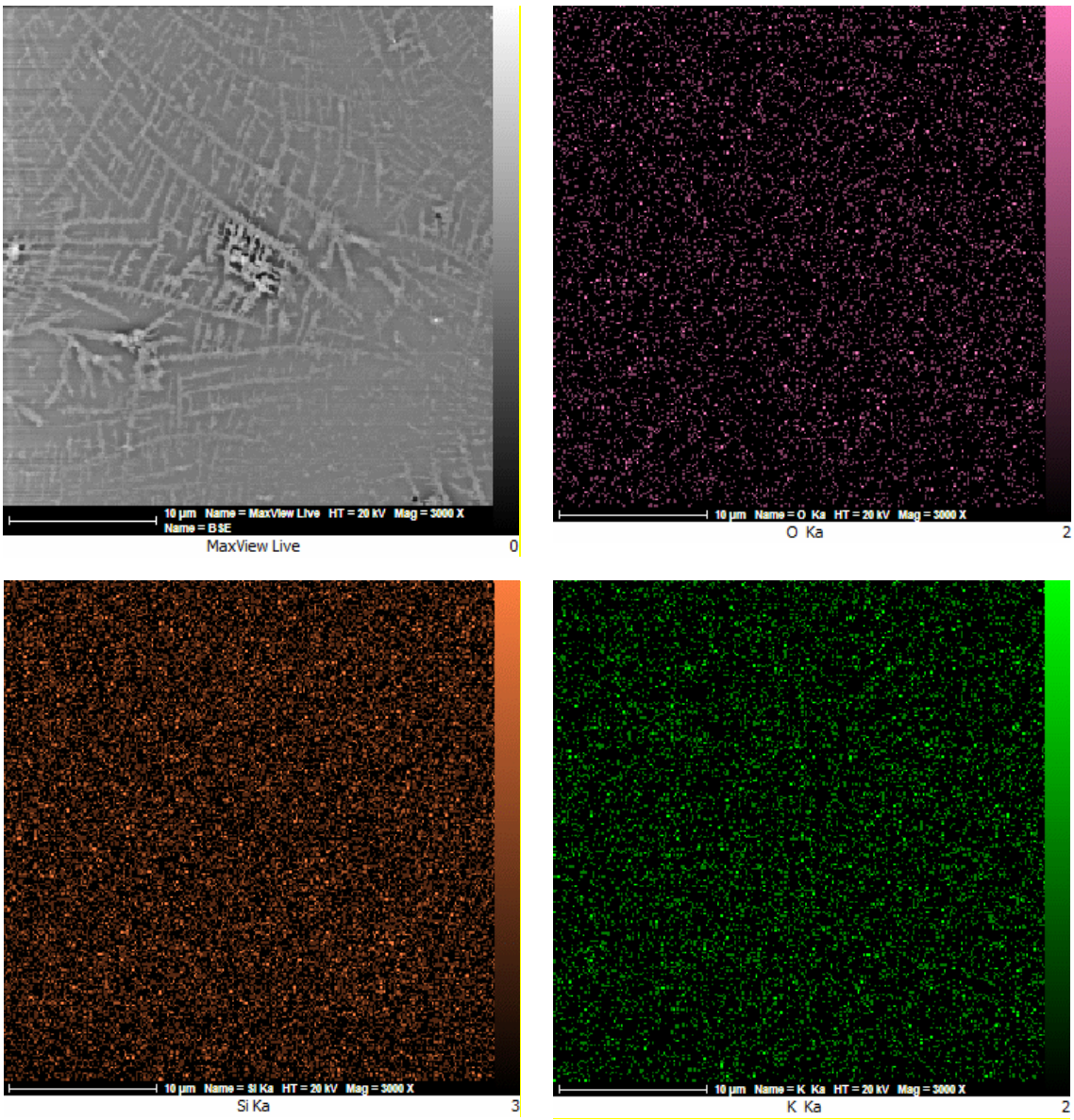

Fig. 13. Map analysis of silicate coating with ratio 2.9. Coating was prepared by 7 min immersion time and then curing in 150°C for 30 min

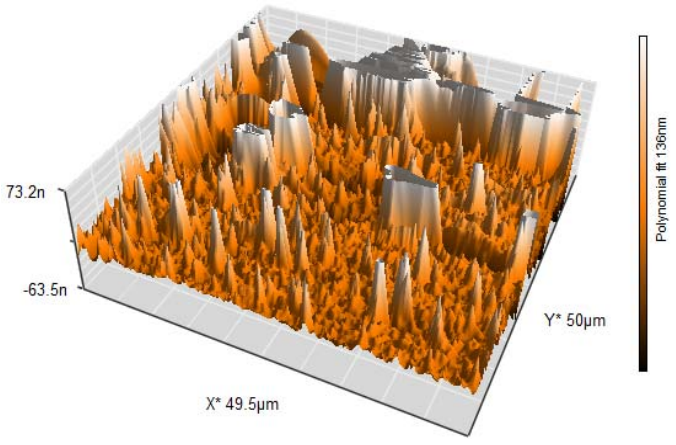

Fig. 14. AFM image of silicate coating with ratio 1.7. Coating was prepared by 7 min immersion time and then curing in 150°C for 30 min

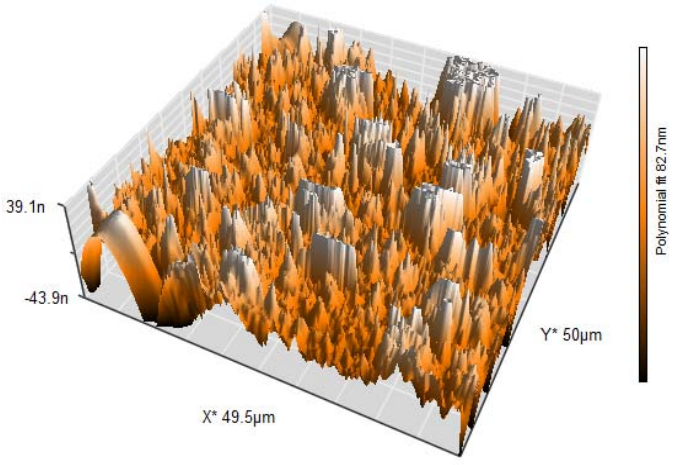

Fig. 15. AFM image of nano-modified silicate coating with ratio 2.9. Coating was prepared by 7 min immersion time and then curing in 150°C for 30 min

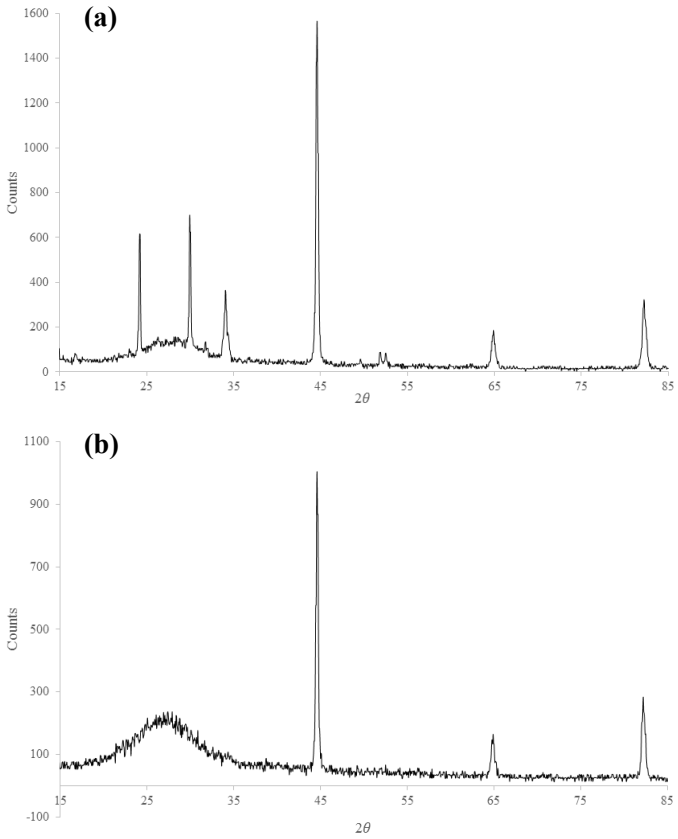

Fig. 16. Normal XRD spectrum of silicate coatings with ratio (a) 1.7, and (b) 2.9. Coating was prepared by 7 min immersion time and then curing in 150°C for 30 min

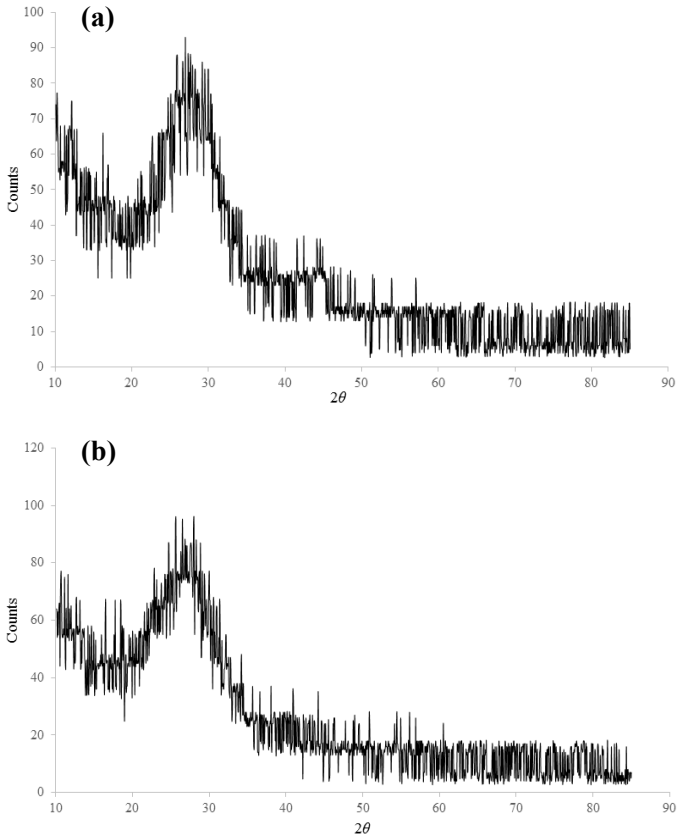

Fig. 17. GIXRD patterns of silicate coatings with ratio (a) 1.7, and (b) 2.9. Coating was prepared by 7 min immersion time and then curing in 150°C for 30 min

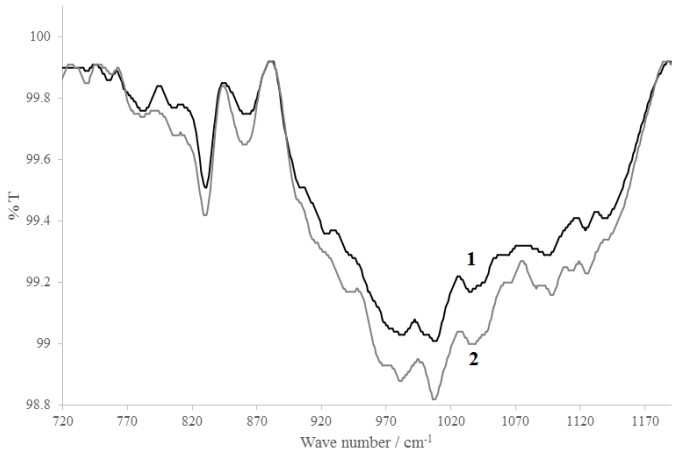

Fig. 18. ATR-FTIR spectra of silicate coatings with ratio (1) 1.7, and (2) 2.9. Coating was prepared by 7 min immersion time and then curing in 150°C for 30 min

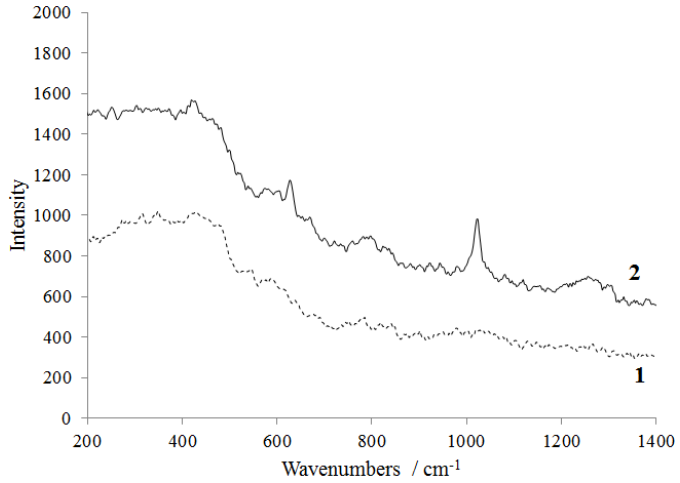

Fig. 19. Raman spectroscopy of silicate coatings with ratio (1) 1.7, and (2) 2.9. Coating was prepared by 7 min immersion time and then curing in 150°C for 30 min

TABLE 4

Electrochemical parameters of nano-modified silicate coating in 3.5 wt.% NaCl solution. Coatings were prepared by immersion in solution with ratio 2.9 for 7 min and then 30 min drying in different temperatures

Drying temperature	E_{corr} / V	I_{corr} / A cm^{-2}	β_a / V dec^{-1}	β_c / V dec^{-1}	R_p / Ohm	V_{corr} / mm y^{-1}
50°C	–0.573	7.71×10^{-9}	0.064	0.065	$1.82\times10^{+6}$	8.381×10^{-5}
100°C	–0.452	6.79×10^{-10}	0.046	0.056	$1.62\times10^{+7}$	7.391×10^{-6}
150°C	–0.785	9.49×10^{-11}	0.073	0.07	$1.63\times10^{+8}$	1.033×10^{-6}
200°C	–0.487	1.65×10^{-10}	0.06	0.056	$7.61\times10^{+7}$	1.799×10^{-6}

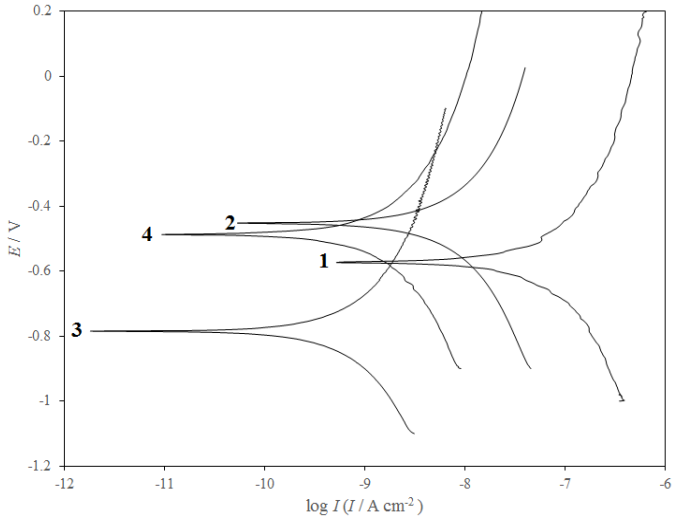

Fig. 20. Polarization curves of nano-silicate coating in 3.5 wt.% NaCl solution. Coatings were obtained by immersion in solution with ratio 2.9 for 7 min and then 30 min drying in different temperatures: (1) 50°C, (2) 100°C, (3) 150°C, and (4) 200 °C

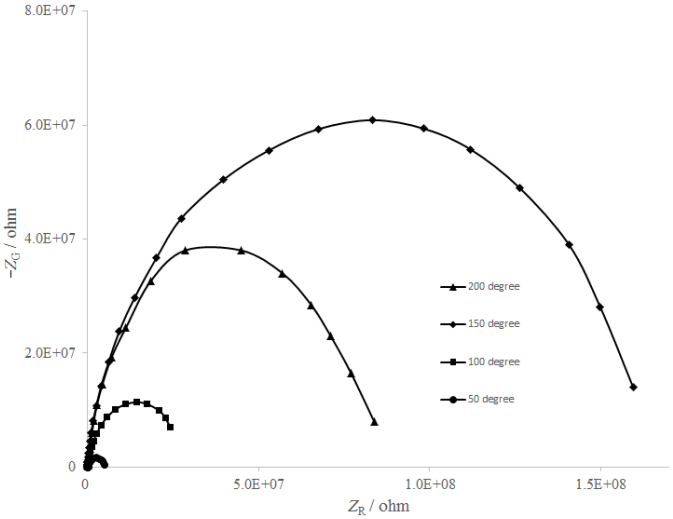

Fig. 21. Electrochemical impedance spectroscopy diagrams of nano-silicate coating in 3.5 wt.% NaCl solution. Coatings were obtained by immersion in solution with ratio 2.9 for 7 min and then 30 min drying in different temperatures: (1) 50°C, (2) 100°C, (3) 150°C, and (4) 200°C

sion rate of the coated samples decrease by increasing curing temperature from 50 to 150°C. Therefore, the optimum drying temperature is obtained at 150°C which related to the compact structure of silicate coating. In addition, it can be concluded that the 150°C drying temperature is sufficient for a dense cross-linked silicate coating formation. In heat treatment temperatures at 50 and 100°C, lower cross-linked silicate film is created. In higher drying temperature around 200°C, the corrosion resistance decreases because at this temperature, high rate of water evaporation causes to the formation of more cracks on the surface.

Impedance plots for nano-silicate coatings obtained at different drying temperature are shown in Fig. 21 and the corresponding parameters are illustrated in Table 5. Silicate coatings indicate capacitive arc attributed to the polarization resistance and the double layer capacitance. As seen, with increasing operating temperature, the polarization resistance enhances and higher polarization resistance is obtained by 150°C drying temperature.

TABLE 5

Electrochemical impedance parameters of nano-modified silicate coating in 3.5 wt.% NaCl solution. Coatings were prepared by immersion in solution with ratio 2.9 for 7 min and then 30 min drying in different temperatures

Curing temperature	Q_{dl} / F	R_{ct} / Ω	n
50°C	4×10^{-9}	$5.09\times10^{+6}$	0.76
100°C	2×10^{-8}	$2.85\times10^{+7}$	0.87
150°C	9×10^{-9}	$1.68\times10^{+8}$	0.79
200°C	4×10^{-10}	$8.62\times10^{+7}$	0.88

4. Conclusion

Silicate coatings were deposited on low carbon steel by dip immersion method. Silicate coatings contained some drawback such as crack, pore and agglomerates and these caused to have low corrosion resistance. Therefore, necessity to modification was obvious. The modification and strengthening of silicate was done by loading colloidal nano-particles into the coatings. Nano silicate coatings showed higher corrosion resistance and barrier property. Nano incorporation caused to decrease the defect and so faultless layer can be achieved by loading optimum amount of nano into the coating. The effects of nano-content and drying temperature on corrosion resistance were investigated. According to experimental data, nano-modified coating with ration 2.9 which dried for 30 min at 150°C showed the best corrosion performance. FESEM and AFM revealed that surface of nano-modified coatings are uniform with low cracks and agglomerates. GIXRD, ATR-FTIR and Raman analysis of coatings indicated that the silicate and nano loaded silicate coatings were amorphous and the siloxane bridges were increased in the presence of colloidal nano silica.

REFERENCES

[1] T. Węgrzyn, J. Piwnik, Z. Stanik, D. Węgrzyn, D. Sieteski, Arch. Metall. Mater. **62**, 1647 (2017).
[2] M. Rozmus-Górnikowska, M. Blicharski, Arch. Metall. Mater. **62**, 787 (2017).
[3] M. Scendo, N. Radek, J. Konstanty, K. Staszewska, Arch. Metall. Mater., **61**, 1895 (2016).
[4] P. Ledwig, M. Kot, T. Moskalewicz, B. Dubiel, Arch. Metall. Mater. **62**, 405 (2017).
[5] N. Gidikova, M. Sulowski, V. Petkov, R. Valov, G. Cempura, Arch. Metall. Mater. **62**, 2421 (2017).
[6] B. Szczucka-Lasota, J. Piwnik, Arch. Metall. Mater. **62**, 1499 (2017).
[7] H. R. Zamanizadeh, M. R. Shishesaz, I. Danaee, D. Zaarei, Prog. Org. Coat. **78**, 256 (2015).

[8] F. Tohidi Shirehjini, I. Danaee, H. Eskandari, D. Zarei, J. Mater. Sci. Technol. **32**, 1152 (2016).
[9] P. Ledwig, B. Dubiel, Arch. Metall. Mater. **62**, 2455 (2017).
[10] T. Ratajski, I. Kalemba-Rec, B. Dubiel, Arch. Metall. Mater. **62**, 2073 (2017).
[11] A. Montiel-García, E. Onofre Bustamante, M.L. Escudero-Rincón, E.C. De la Cruz-Terrazas, A.M. Torres-Huerta, Cement Concrete Comp. **90**, 202 (2018).
[12] M.R. Majdi, I. Danaee, S.S. Seyyed Afghahi, Mater. Res.-Ibero-Am. J. **20**, 445 (2017).
[13] V. Asadi, I. Danaee, H. Eskandari, Mater. Res.-Ibero-Am. J. **18**, 706 (2015).
[14] M. Kazemi, I. Danaee, D. Zaarei, Mater. Chem. Phys. **148**, 223 (2014).
[15] H. Bahri, I. Danaee, G. R. Rashed, Surf. Coat. Technol. **254**, 305 (2014).
[16] H. Bahri, I. Danaee, G.R. Rashed, A.R. Dabiri, Mater. Sci. Technol. **32**, 1346 (2016).
[17] G. Parashar, M. Bajpayee, P.K. Kamani, Surf. Coat. Int. Coat. Trans. **86**, 209 (2003).
[18] J.L. Bass, G.L. Turner, J. Phys. Chem. B. **101**, 10638 (1997).
[19] T. Hiemstra, M.O. Barnett, W.H. van Riemsdijk, Interaction of silicic acid with goethite, J. Colloid Interf. Sci. **310**, 8 (2007).
[20] N. Jordan, N. Marmier, C. Lomenech, E. Giffaut, J.J. Ehrhardt, J. Colloid Interface Sci. **312**, 224 (2007).
[21] X. Yang, P. Roonasi, A. Holmgren, J. Colloid Interf. Sci. **328**, 41 (2008).
[22] L.A. Garcia-Cerda, O. Mendoza-Gonzalez, J.F. Perez-Robles, J. Gonzalez Hernandez, Mater. Lett. **56**, 450 (2002).
[23] R.P. Socha, J. Fransaer, Thin Solid Films **488**, 45 (2005).
[24] M.R. Yuan, J.T. Lu, G. Kong, C.S. Che, Surf. Coat. Technol. **205**, 4507 (2011).
[25] V. Palanivel, D. Zhu, W.J. Ooij, Prog. Org. Coat. **47**, 384 (2003).
[26] H. Bahri, I. Danaee, G.R. Rashed, D. Zaarei, J. Mater. Eng. Perform. **24**, 839 (2015).
[27] D. Zhu, W.J. Ooij, Corros. Sci. **45**, 2177 (2003).
[28] R. Gaggiano, P. Moriamé, M. Biesemans, I. De Graeve, H. Terryn, Surf. Coat. Technol. **205**, 5210 (2011).
[29] W.J. Van Ooij, D. Zhu, M. Stacy, A. Seth, T. Mugada, J. Gandhi, P. Paomi, Tsinghua Sci. Technol. **10**, 639 (2005).
[30] M. Quinet, B. Neveu, V. Moutarlier, P. Audebert, L. Ricq, Prog. Org. Coat. **58**, 46 (2007).
[31] S. Darwich, M.Sc. thesis, Corrosion protection concepts for aluminium and magnesium alloys coated with silica films prepared by water-based sol-gel process, Technischen Universitat Chemnitz, 2012.
[32] H. Bahri, I. Danaee, G.R. Rashed, Mater. Test. **57**, 402 (2015).
[33] F. Jamali, I. Danaee, D. Zaarei, Mater. Corros. **66**, 459 (2015).
[34] M. Rokita, W. Mozgawa, A. Adamczyk, J. Mol. Struct. **1040**, 125 (2014).
[35] X. Yang, P. Roonasi, R. Jolsterå, A. Holmgren, Colloids Surf. A Physicochem. Eng. Asp. **343**, 24 (2009).
[36] M.R. Yuan, J.T. Lu, G. Kong, Surf. Coat. Technol. **204**, 1229 (2010).
[37] M.R. Yuan, J.T. Lu, G. Kong, C.S. Che, Surf. Coat. Technol. **205**, 4466 (2011).
[38] M. Kobayashi, F. Juillerat, P. Galletto, P. Bowen, M. Borkovec, Langmuir **21**, 5761 (2005).
[39] C.B. Dallam, N. Karogal, United States of America Patent US7147725B2.
[40] S. Dalbin, G. Maurin, R.P. Nogueira, J. Persello, N. Pommier, Surf. Coat. Technol. **194**, 363 (2005).
[41] S. RameshKumar, I. Danaee, M. RashvandAvei, M. Vijayan, J. Mol. Liq. **212**, 168 (2015).
[42] A. Karimi, I. Danaee, H. Eskandari, M. RashvanAvei, Prot. Met. Phys. Chem. Surf. **51**, 899 (2015).
[43] D. Singh, R. Kumar, A. Kumar, K.N. Rai, Cerâmica **54**, 203 (2008).
[44] N. Lari, S. Ahangarani, A. Shanaghi, Optik **126**, 5363 (2015).
[45] L. de Ferri, P.P. Lottici, A. Lorenzic, A. Monteneroc, E. Salvioli-Mariani, J. Cultural Heritage **12**, 356 (2011).
[46] C. Domingo, M. A. de Buergo, S. Sanchez-Cortes, R. Fort, J.V. Garcıa-Ramos, M. Gomez-Heras, Prog. Org. Coat. **63**, 5 (2008).